J. Fluid Mech. (1985), vol. 160, pp. 137–154
Printed in Great Britain

Time-dependent convective instabilities in a closed vertical cylinder heated from below

By J. R. ABERNATHEY† and F. ROSENBERGER
Departments of Physics, and Materials Science and Engineering, University of Utah, Salt Lake City, UT 84112

(Received 27 August 1984 and in revised form 13 May 1985)

The convective behaviour of xenon gas in a vertical thermally conducting cylinder (height/radius = 6) heated from below was investigated. Convectively induced temperature fluctuations in the gas were analysed with digital signal-processing techniques over a range of Rayleigh number $0 \leqslant Ra \lesssim 2300$. Quiescent, steady-state, periodic and weakly turbulent convective regimes were characterized. Bistability of steady states (mode switching) was observed in the range $400 \lesssim Ra \lesssim 700$. At $Ra = 1550$ a strictly periodic flow developed. With increasing Ra two additional incommensurate frequencies appeared, leading to 'turbulence' at $Ra \approx 2000$. This turbulence, characterized by a broadband power spectrum, intermittently showed periodic flow. A periodic window with a period-doubling sequence appeared between $2100 \lesssim Ra \lesssim 2200$. The spectral features of this sequence can be followed into the broad band noise at higher Ra. Although these experiments were conducted quasistatically, a strong hysteresis was observed with decreasing Ra. Furthermore, it was demonstrated that the sequence of convective regimes can be fundamentally altered by *minor* perturbations (self-heating) from the flow sensors.

1. Introduction

There is a large body of experimental work on the convective instabilities of free convection (for an overview see e.g. Normand, Pomeau & Velarde 1977). Most of this work has been concerned with fluids of either high or low Prandtl number Pr. However, the behaviour of gases ($Pr \approx 1$) in vertical cylinders has been addressed by only a few experimentalists. Mitchell & Quinn (1966) performed the first detailed investigation of such systems. They detected transitions between steady-state convection modes from smoke traces and from abrupt changes in local temperature. They also observed periodic and chaotic convective behaviour at high Rayleigh numbers Ra.

In order to more closely simulate the conditions of closed-ampoule vapour crystal-growth systems, Olson & Rosenberger (1978*a*, *b*) performed experiments with various gases in a cylindrical convection cell of small aspect ratio. They obtained good agreement with the theoretically predicted Ra^{cr} at the onset of convection. In addition, they observed higher-mode transitions, including the development of turbulent flow. We have continued their work with an emphasis on the quantitative characterization of oscillatory flow and its transition to turbulent behaviour.

In lieu of a quantitative theory of the transition to turbulence, several conjectures have been put forth, often from very different points of view. Recently, several

† Present address: IBM Corporation, General Technology Division, Essex Junction, VT 05452.

excellent reviews have synthesized and cataloged the principal features of these conjectures (Swinney & Gollub 1981; Velarde 1981, Eckmann 1981). Hence we will here outline only the essential features of the four most commonly discussed models for comparison with our experimental results.

The Landau–Hopf picture of turbulence (Landau & Lifshitz 1978; L'vov & Predtechensky 1981) can be illustrated by considering linearized disturbances to steady-state solutions f_0 of the Navier–Stokes equations. Denoting a disturbance vector f_1, separation of variables gives the time dependence as

$$f_1 = e^{(\omega - i\gamma)t} f_{1\omega}(x)$$

The complex eigenfrequencies $\omega - i\gamma$ determine the bifurcation to time-dependent behaviour. When Ra is increased sufficiently one eigenfrequency $\omega_1 - i\gamma_1$ crosses the real axis and f_0 becomes unstable against perturbations of frequency ω_1. For $Ra > Ra^{cr}$ the solution is no longer the steady flow f_0 but rather time-dependent with frequency ω_1 (if $\omega_1 = 0$ then the flow bifurcates to a new steady state). Such a time-dependent instability is known as a Hopf bifurcation (Hirsch & Smale 1974). Landau speculated that as Ra is increased above Ra^{cr} a similar analysis for the mean part of the new time-dependent flow will produce a second Hopf bifurcation to a frequency ω_2. The process would occur *ad infinitum* as $Ra \to \infty$. At each bifurcation a new incommensurate frequency would appear with arbitrary phase. The solution $f(t)$ would then have the form

$$f(t) = f(\omega_1 t + \alpha_1, \omega_2 t + \alpha_2, \omega_3 t + \alpha_3 \ldots \omega_n t + \alpha_n),$$

with

$$n \to \infty \quad \text{as} \quad Ra \to \infty.$$

One criticism of the Landau–Hopf conjecture is that these quasiperiodic (multiply periodic) solutions do not phase-mix (Hirsch & Smale 1974). The property of phase-mixing can be expressed by the condition

$$R(\tau) = \lim_{T \to \infty} \int_0^T f(t+\tau) f(\tau)\, dt \to 0 \quad \text{as} \quad \tau \to \infty,$$

where $R(\tau)$ is the autocorrelation function. This means that the values of the quasiperiodic functions at two distant times are correlated as 'strongly' as at two close times. A non-vanishing autocorrelation at long time delays is contrary to both experimental evidence and to an intuitive concept of the nature of turbulence (Velarde 1981; Eckmann 1981).

Another possible criticism of the Landau–Hopf conjecture was raised by Ruelle & Takens (1971). They have shown that for a large class of differential equations, after (typically) three Hopf bifurcations producing three incommensurate frequencies, the phase-space trajectories may orbit about a 'strange attractor'. This implies that after the appearance of the third bifurcation the power spectrum $P(\omega)$ of $f(t)$ becomes broadband, i.e. discrete frequencies give way to a distribution of frequencies over a finite band in the spectrum, thus giving it the appearance of noise.

Another conjecture about the transition to turbulence was put forth by Feigenbaum (1979). Its main feature is that after a single Hopf bifurcation to a frequency ω_1, n successive period-doubling (subharmonic) bifurcations to frequencies $2^{-n}\,\omega_1$ occur. The ΔRa between successive bifurcations becomes smaller as n increases. At $n = \infty$ an accumulation point Ra_∞ = finite is reached, uniquely defining the onset of turbulence. Simple one-dimensional nonlinear systems can have periodic 'windows' within the turbulent (chaotic) regime that evolved through a Feigenbaum sequence

(May 1976). Such a period-doubling route to turbulence, with narrow periodic windows within the chaotic regime, has most recently been obtained in numerical experiments on two-dimensional thermosolutal convection by Moore *et al.* (1983).

Finally, another conjecture was proposed by Pomeau & Manneville (1980); see also Hirsch, Huberman & Scalapino (1982). Briefly stated, their scenario has a periodic solution (i.e. with only one or a few fundamental frequencies) becoming turbulent through intermittency. As Ra is increased, turbulent (noisy) 'bursts' occur intermittently between times of periodic or steady-state behaviour. The length of time between the turbulent bursts shortens and their duration increases as Ra is increased. Pomeau & Manneville propose that there is a critical Ra^{cr} at which the bursts first occur. The conjecture predicts an exponential relation of the mean time τ_l between turbulent bursts to Ra of the form

$$\tau_\ell \propto (Ra - Ra^{cr})^{-(1/z-1)},$$

where z is a constant determined by the specific fluid system.

2. Experimental technique

The convection cell, heating arrangement, temperature stability, and the gas-filling and Ra-determination procedures were the same as reported earlier by Olson & Rosenberger (1978*a*). Xenon gas (density $\rho = 8 \times 10^{-3}$ g/cm^3) was used throughout.

Figure 1 illustrates schematically the thermometric technique used in our study. Two microthermistors (bead diameter $\leqslant 0.2$ mm, lead diameter 25 μm) oppositely arranged in the midplane of the convection cell, protrude a few millimetres into the gas. In a quiescent fluid, i.e. for $Ra < Ra^{cr}$, isotherms form horizontal planes. Thus the temperature difference between the probes $2T' = 0$. Any asymmetric flow, however, results in a finite $2T'$, which can be detected in a differential bridge circuit (figure 1*a*). The resolution in $2T'$ with this differential arrangement was better than 0.0002 °C. For the study of time-dependent convection, where temperature fluctuations about a mean were of the main interest, the thermistor probes were arranged in a single-ended bridge circuit (figure 1*b*). With the differential measurements, changes of the average temperature were effectively locked-out; average temperature changes in the singled-ended measurements, however, caused d.c. offsets, which required occasional rebalancing of the bridge.

The thermistor bridge signal was buffered through a highly stable differential amplifier and a 3-pole tuneable bandpass filter set to 2 Hz bandwidth, to remove 60 Hz line noise. This high-level signal was connected to the data-acquisition board of a microcomputer and a chart recorder, as indicated schematically in figure 2.

At a given Ra, n samples of the signal were stored on a disc. For the detection of transitions between modes, n was usually 200. For power-spectral calculations, either $n = 2048 = 2^{11}$ or $4096 = 2^{12}$ samples were taken and stored. At each Ra we calculated from the samples the mean μ and the deviation σ, defined by

$$\mu = \frac{1}{n} \sum_{i=1}^{n} 2T'(i),$$

$$\sigma^2 = \frac{1}{n} \sum_{i=1}^{n} [2T'(i) - \mu]^2.$$

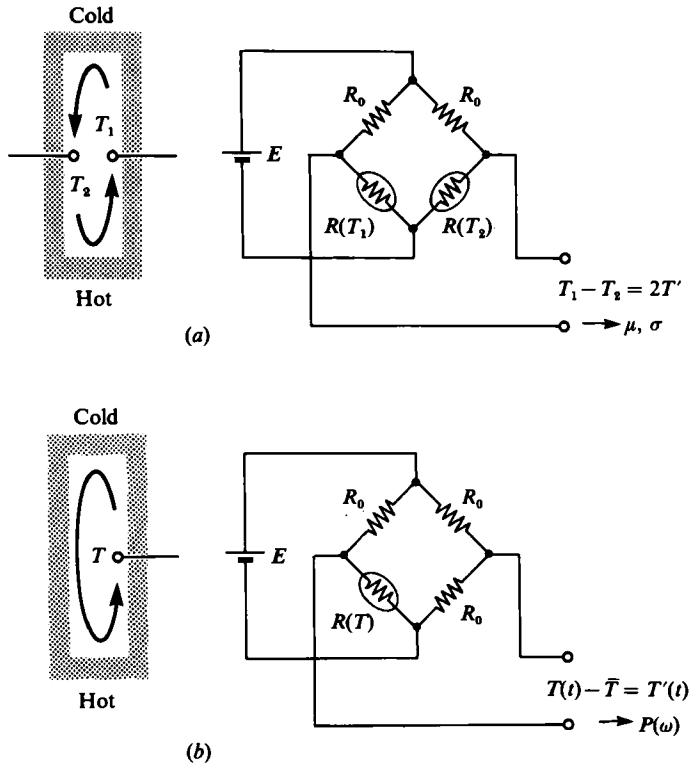

FIGURE 1. Thermistor-bridge circuits: (*a*) differential temperature measurements; (*b*) single-ended temperature measurements.

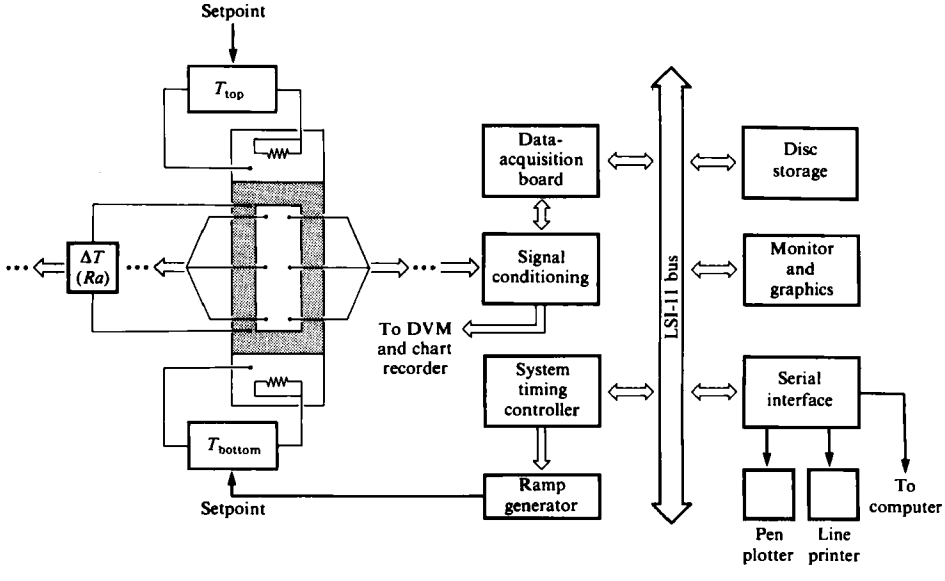

FIGURE 2. Schematic diagram of digital signal-processing system used in convection experiments.

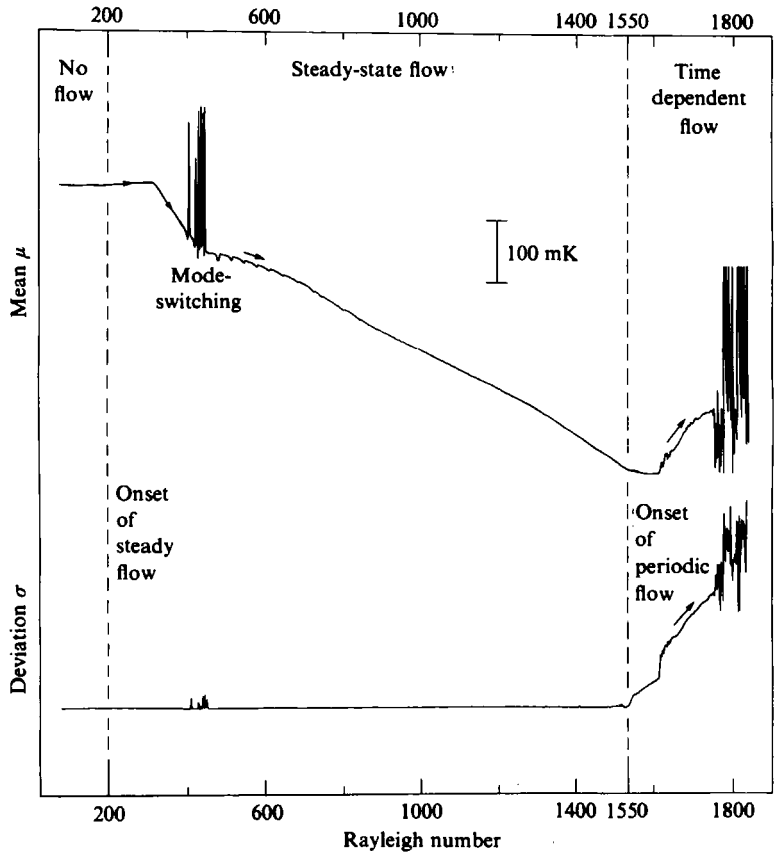

FIGURE 3. Mean μ and deviation σ of $2T'$ versus Ra for increasing Rayleigh number. See text for interpretation.

If the convective mode is steady-state, then $\mu = 2T'$ and $\sigma = 0$; with μ changing with the amplitude of the mode. However, if convection becomes time-dependent, σ becomes non-zero and μ indicates the average (or d.c.) character of the flow.

Power spectra were calculated after subtracting the mean from the data to avoid a large d.c. spectral peak. The data were then multiplied by a discrete Hamming window for leakage reduction (Rabiner & Gold 1975) and processed through a fast-Fourier-transform program (Brigham 1974). Each set of data was normalized to the highest peak in its spectrum, and the logarithm at each sample frequency was computed so that the spectra could be displayed in dB. Spectra were drawn by a pen plotter and peaks were identified by editing the spectra on a graphics monitor.

After sufficient data were acquired, Ra was automatically changed by a small programmed amount. This was followed by a programmed settling time to allow the flow to reach the state characteristic of the new Rayleigh number. The 'resolution' and 'scan rate' were thus determined by the size of the Rayleigh number steps ΔRa and the settling time τ_{set}. A detailed description of the detection system, including the digital signal-processing circuitary and data acquisition system has been given elsewhere (Abernathey 1982).

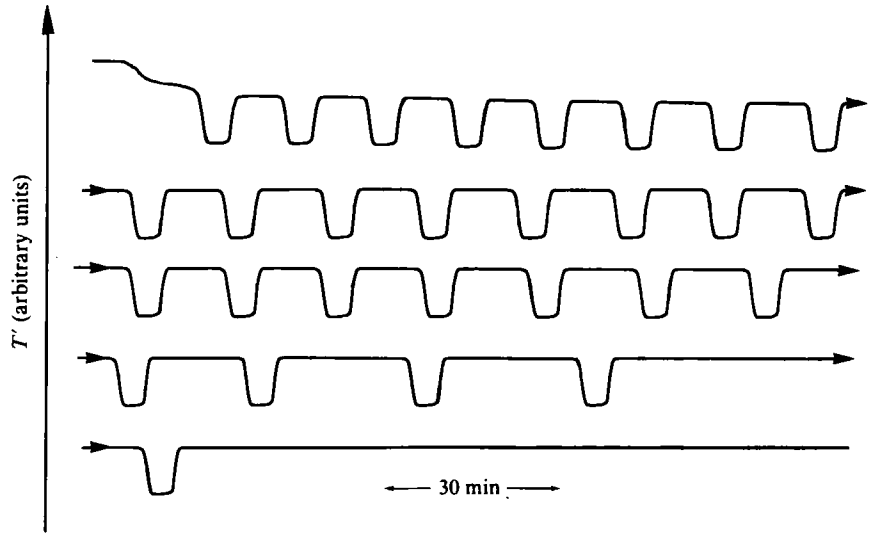

FIGURE 4. Switching between steady-state convection modes ($Ra \approx 400$–700).

3. Experimental results and discussion

3.1. *Steady states and the onset of time-dependent convection*

Figure 3 shows μ and σ plotted versus Ra for the range $6 \leqslant Ra \leqslant 1828$ with $Ra \propto r^4/h$, where r is the radius and h the height of the cell. This scan was performed in steps of $\Delta Ra \approx 1.5$ and with a settling time $\tau_{set} = 20$ min. For comparison, the thermal diffusion time ($\tau_t = l^2/\kappa$) was $\tau_t^{vert} = 15$ min for the cell height and $\tau_t^{hor} = 25$ s for the cell radius. Such a long settling time was required since $\tau_{set} = 5$ min was found to lead to 'smearing' of some of the features shown in figure 3. From the $\mu(Ra)$ curve one sees that convection sets in at $Ra \approx 200$, which corresponds to $\Delta T = 0.55$ °C. This Ra^{cr} agrees reasonably well with earlier measurements and theoretical predictions (Olson & Rosenberger 1978*a*). An unexpected feature, however, is the presence of large 'spikes' at $Ra \approx 470$–490. The slope of $\mu(Ra)$ changes on either side of the spikes, indicating that a change in the global flow pattern occurred in this range. In addition, the deviation σ also has small but non-zero values at the same Ra-values as the μ-spikes. Apparently, the transition between these two stable steady states (flow patterns) does not occur at a unique value of Ra.

Figure 4 shows $2T'(t)$ recorded during an earlier experiment with Kr gas in which the imposed Ra had just been abruptly changed from 700 to about 400, i.e. through the range of spikes in figure 3. Both the Ra and the frequency of these pulses are much lower than those observed for continuous oscillatory convection in previous slow-scan experiments (Olson & Rosenberger 1978*a*). We tentatively assign the pulses, together with the spikes in figure 3, to a switching between bistable states. Rosenblat (1982) has predicted bistable steady-states above Ra^{cr} for free convection in vertical cylinders. Behringer & Ahlers (1982) observed slow-timescale steady-state switching in liquid helium in a cylinder of somewhat larger aspect ratio r/h than ours at $Ra/Ra^{cr} \approx 3.4$–3.5. This is fairly close to the values of $Ra/Ra^{cr} \approx 2.4$–3.2 observed in our experiments. The decaying of the pulse 'firing rate' in figure 4 is most likely a result of the transient response to the large ΔRa.

For higher Ra figure 3 shows that $\mu(Ra)$ continues with relatively constant slope up to $Ra \approx 1550$. At this value σ begins to deviate from zero and grows with Ra.

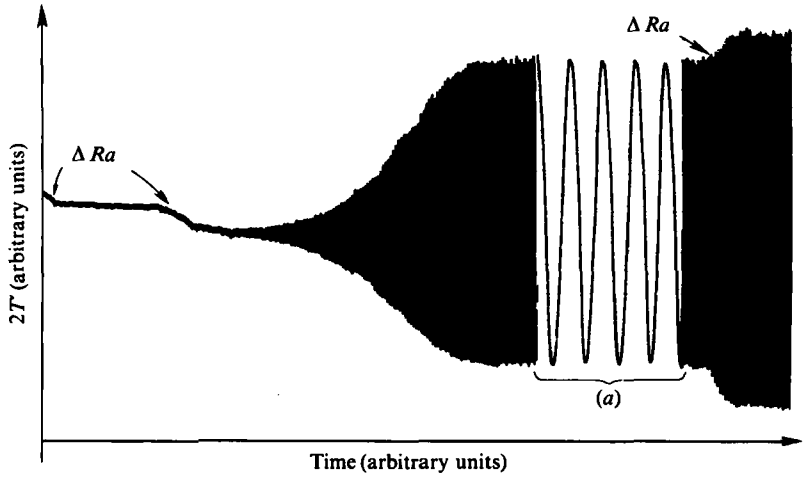

FIGURE 5. The onset of time-dependent convection: stripchart recording of differential temperature $2T'$. The timescale has been expanded over the interval (a) to show the sinusoidal character of the waveform. Increases in Ra ($\Delta Ra \approx 75$) are marked.

This indicates the transition to continuous time-dependent flow, to be investigated in detail in §3.2. It appears that this time dependence begins as a fluctuation riding on top of the mean flow. However, the mean flow changes its form at $Ra \approx 1620$ as indicated by the discontinuities in both curves at that Rayleigh number. Other discontinuities occur before the breakdown at $Ra \approx 1750$.

3.2. *Time-dependent convection and the transition to turbulence*

3.2.1. *Power-spectral presentation of convective temperature fluctuations*

We performed several series of experiments designed to study time-dependent convection and the transition to turbulence. The goal was to determine the dynamical behaviour of convection as a single parameter, the Rayleigh number, was varied. In addition, we hoped to verify experimentally the applicability of one or more of the conjectures on the transition to turbulence outlined above.

Our method of analysis is based on recording the time history of local temperature fluctuations. A direct recording (waveform) of the time history $f(t)$ and its calculated power spectrum $P(\omega)$ were the main tools of our analysis (see e.g. Rabiner & Gold 1975; Brigham 1974). An experimental series consisted of many such time history analyses performed over a range of Rayleigh numbers (i.e. a scan).

Figure 5 shows a recorded trace of the local temperature of a probe in a convection cell. Changes in Rayleigh number are reflected in changes in the d.c. value of the signal. When the critical value of $Ra = Ra^{\mathrm{osc}}$ is reached oscillations develop with an amplitude that exponentially increases with time. The amplitude of the oscillations eventually saturates to a specific value that depends on Ra. In figure 5 the timescale is expanded over an interval to show the sinusoidal character of the waveform. Such an oscillation at a frequency f gives a power spectrum with a single sharp (delta-function) peak.

In the following figures we have normalized the value of the actual Ra of a given experiment to the value of $Ra^{\mathrm{osc}} = 1550$. The parameter $R = Ra/Ra^{\mathrm{osc}}$ is thus 1.000 at the onset of oscillations. However, a close examination of high-resolution power spectra indicates that a small but distinct peak appears at lower values of R than

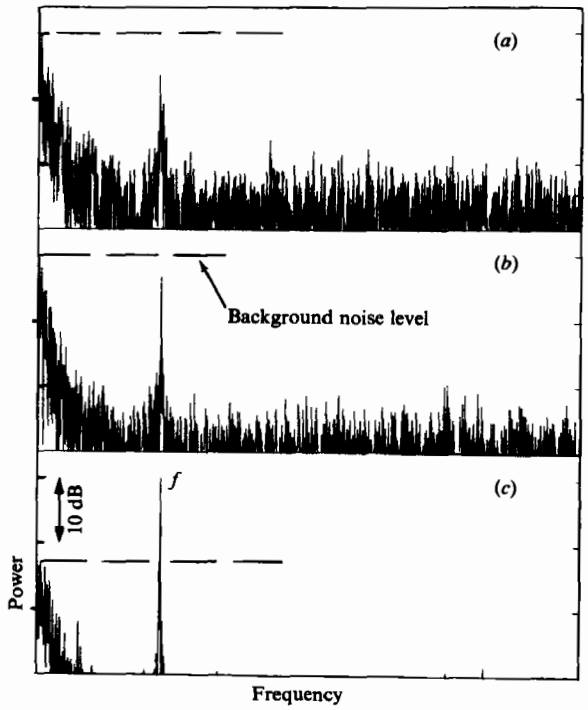

FIGURE 6. Power spectra of $T'(t)$ at (*a*) $R = 0.9974$; (*b*) 0.9987; (*c*) 1.000. (Normalized to the highest peak in each spectrum.)

can be seen from a chart recording of the signal. Therefore, our operational definition of $R = 1.000$ is when the oscillatory spectral peak becomes larger than any peaks in the back-ground noise spectrum. The development of the sharp spectral peak out of background noise is shown in figure 6.

At each value of R, 4096 digital samples of $f(t)$ were collected. High-resolution spectra were calculated by windowing and then directly Fourier-transforming the entire 4096 data points collected at each Ra. Here we show only a few selected spectra, along with a section of the actual recorded wave-form from which they were calculated, to identify the spectral features (frequencies, coupling, etc.). A large number of spectra, more closely spaced in Ra, have been presented by Abernathey (1982). All spectra show power levels 60 dB below the highest peak in each individual spectrum. Thus the background level is variable, but more low-level spectral features are apparent.

3.2.2. *The up–down scan*

In the first series of experiments, up-scanning (i.e. increasing Rayleigh number scanning) was followed by down-scanning through the same R-range. The ΔR step size was approximately 0.003 and the settling time was 20 min. A total of 275 waveforms (time histories) were recorded at discrete Rayleigh numbers in the up–down series. Each experimental series required nearly one month. This did not allow for extensive repetition of whole scans. Careful 'spot checks' in form of repeated scans over narrow ΔRa ranges, however, demonstrated reproducibility for identically performed experiments.

Figure 7 summarizes the Ra-dependence of major spectral peak frequencies from

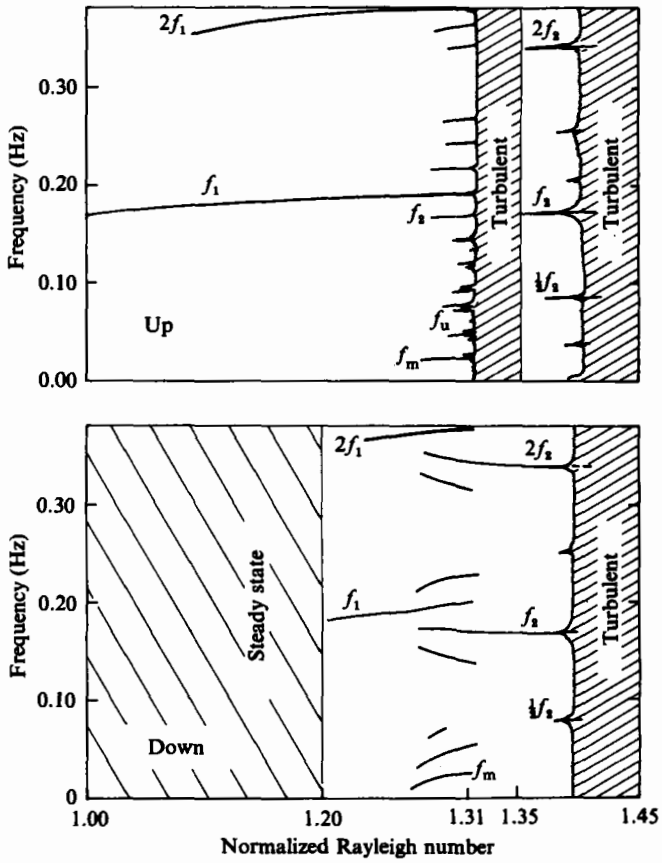

FIGURE 7. Bifurcation diagrams for up and down scans versus R (normalized Rayleigh number).

the up and down scans. The frequency axis extends only to one-half of the Nyquist frequency, so that some of the high harmonics are not shown. Both scans show broadband noise (i.e turbulence) above $R \approx 1.39$. The period-doubled components and broadening are also common to both scans at R just below 1.39 (the onset of turbulence). The major difference, however, is the 'turbulent' region at intermediate values of R (1.316–1.351) which only appears in the up scan. This turbulent region seems to be related to a transition between oscillatory modes. At lower R the fundamental mode oscillates at frequency f_1, but at higher R, where a periodic window re-emerges, f_2 is the fundamental mode. Both the up and down scans show an increased number of sharp spectral peaks in the transition region. However, in the down scan this transition is made by modulation without the flow becoming turbulent.

Some measure of the temperature-fluctuation amplitudes is provided by figure 8. The maximum amplitude $T'_{\max}$ is taken as the difference between maximum and minimum temperature of the entire time history at a given R. Since the large $T'_{\max}$ values resulted from turbulent bursts, we have also plotted, as a more representative measure of the amplitude, the power above background of the highest peak $P_{\max}$ (dashed lines). In contrast with $T'_{\max}$, $P_{\max}$ is relatively constant throughout the turbulent regions investigated.

For a more detailed analysis of the observed routes to and from turbulence,

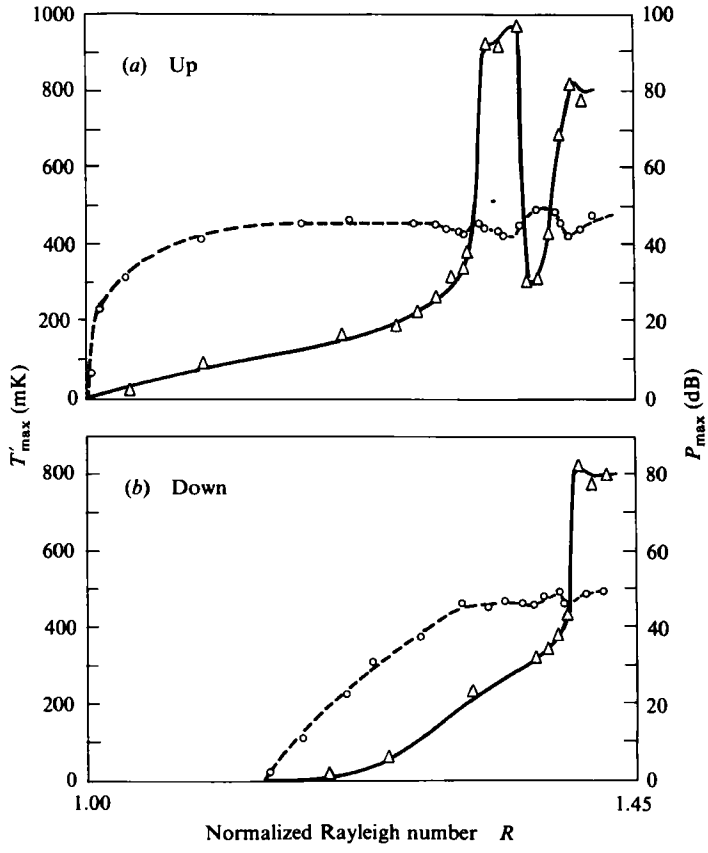

FIGURE 8. Maximum fluctuation amplitude (solid line), and normalized power of highest spectral peak (dashed line) for (*a*) up scan; (*b*) down scan.

through examining the high-resolution spectra, it is helpful to briefly outline the consequences of nonlinear mixing (Marshall 1965). An input of a single harmonic signal $x_1(t)$ into a nonlinearly responding element results in an output that contains higher harmonics of the fundamental frequency ω_1. On input of two oscillatory signals, however, say with ω_1 and ω_m, the nonlinear response results in harmonics of the input fundamentals, and sums and differences (sidebands) of these frequencies: $\omega_1 \pm \omega_m$, $\omega_1 \pm 2\omega_m$, $\omega_1 \pm 3\omega_m$, $2\omega_1 \pm \omega_m$, $2\omega_1 \pm 2\omega_m$, $2\omega_1 \pm 3\omega_m$, $3\omega_1 \pm \omega_m$ etc. Hence the power spectrum of a nonlinearly responding system will show harmonics and sidebands in addition to the fundamental frequencies.

Figure 9 (*a*) shows a power spectrum of the temperature oscillations taken from the up scan. A portion of the recorded waveform is also shown illustrating the strong periodicity. In the spectrum one sees the fundamental frequency f_1 as well as second and third harmonics, which indicates some nonlinearity. The low-frequency noise is part of the narrow bandwidth background.

Figure 9 (*b*) shows the beginning of modulation (or nonlinear mixing). A low frequency modulation f_m appears, resulting in sidebands to f_1 and f_2. We call the lower sidebands $f_1 - f_m = f_2$, which is also approximately the frequency that re-emerges from turbulence in the window at higher R. There is another small noisy peak f_u, which

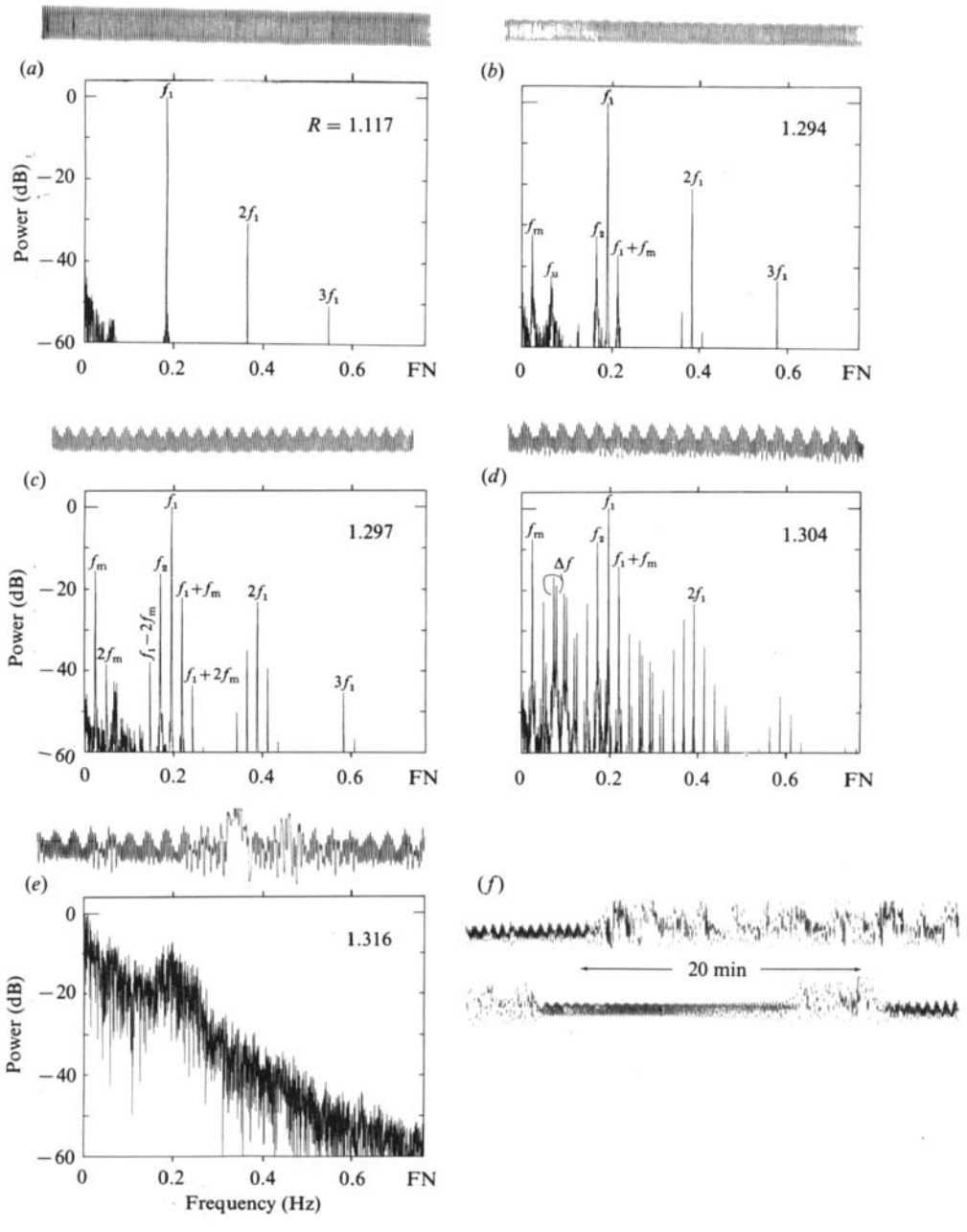

FIGURE 9. (*a*)–(*e*) Selected power spectra and sections of recorded waveform, from up scan. (*f*) Waveform of temperature fluctuations in the weakly turbulent region of the up scan ($R = 1.321$), showing intermittency.

is incommensurate with f_1 and f_m. The waveform faintly shows the 'modulating' envelope corresponding to f_m.

In figure 9(*c*), the modulation frequency f_m is stronger and its second and third harmonics are developed. The modulation envelope is also more discernible in the waveform. The unidentified noisy peak f_u did not increase from figure 9(*b*), and now

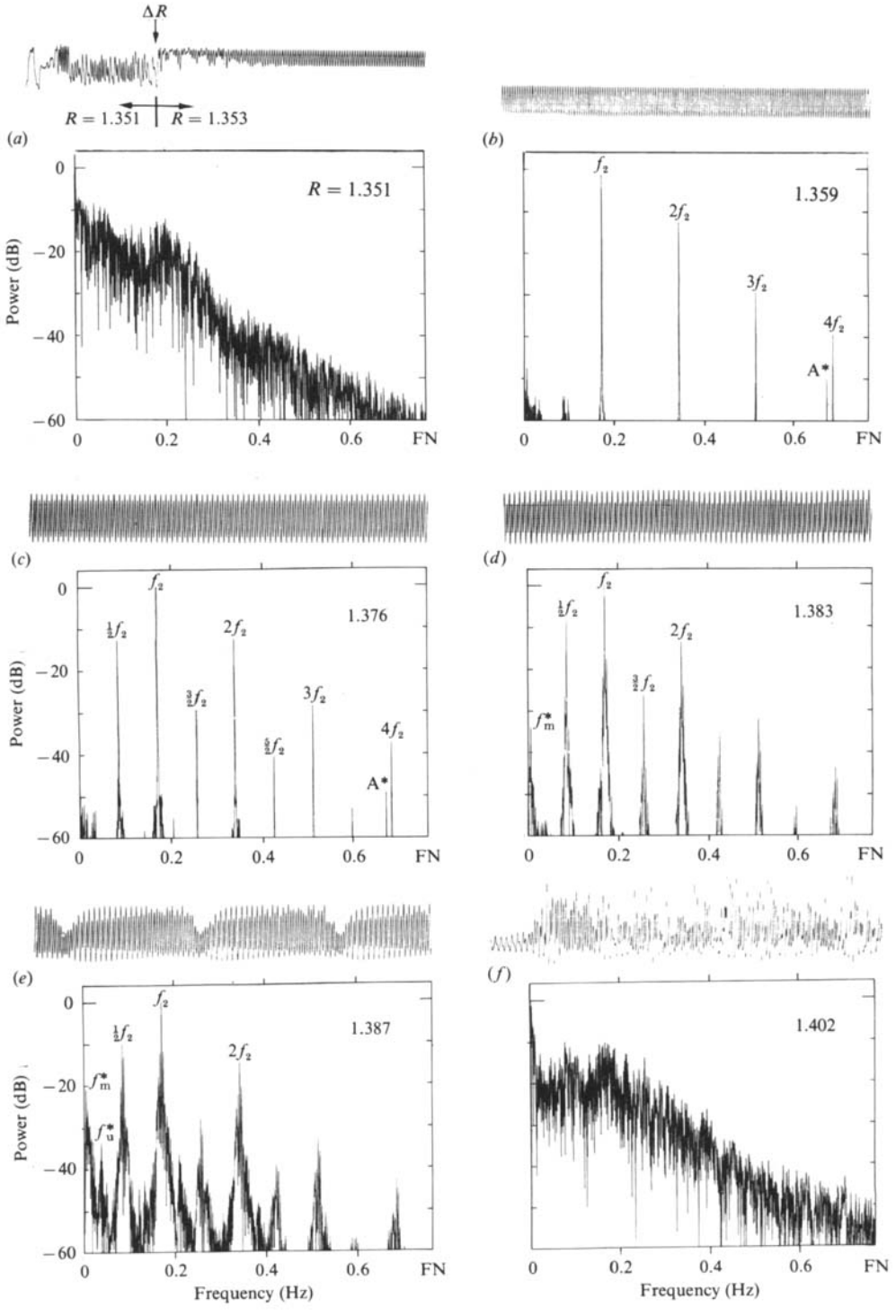

FIGURE 10. Selected power spectra and associated sections of recorded waveform, from up scan.

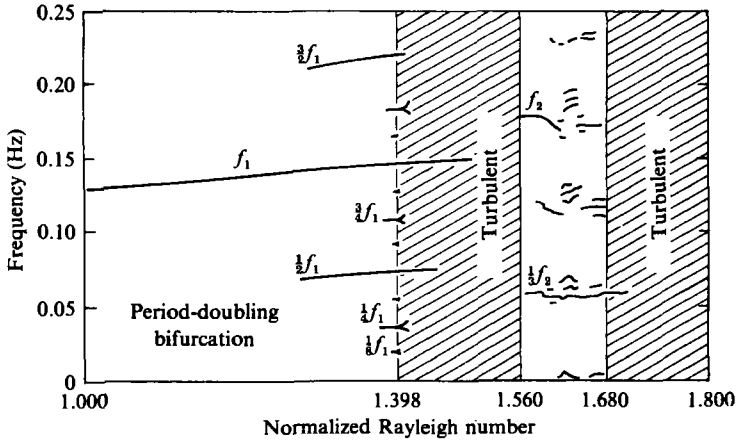

FIGURE 11. Bifurcation diagram showing frequencies versus R from scan with increased sensor self-heating.

is quite near the third harmonic of f_m. Addition sidebands from harmonics of f_m have also developed.

In figure 9(*d*), the modulation development continues, but now f_u 'couples' to the harmonics and sidebands in a curious way. Large 'doublet' peaks with a spacing $\Delta f \sim |f_u - 3f_m|$ emerge in the region between $2f_m$ and $f_1 - 2f_m$ as well as $f_1 + 2f_m$. Another peak emerges halfway between the doublet peaks at $R = 1.310$, and the bases of these peaks are broadened, indicating an increase in noise (Abernathey 1982). The cause of these 'doublet' peaks is not clear, but it is *not* a case of 3-mode modulation since Δf is constant everywhere the doublets occur.

In figure 9(*e*) the spectrum is now noisy, reflecting the onset of weak turbulence, yet examination of a section of waveform for this Rayleigh number shows fairly periodic behaviour (similar to that in figure 9*d*) separated by turbulent 'bursts', i.e. intermittency. A waveform (recorded at $Ra = 1.321$) representative of this intermittency is shown in figure 9*f*. The quasiperiodic intervals between turbulent bursts last as long as twenty minutes. The periodic behaviour becomes less and less frequent as R is increased.

At $R = 1.351$ the waveform contained no discernible periodic sections. However, when R is increased to 1.353 periodicity (frequency f_2) re-emerges. A waveform exhibiting this transition is shown in figure 10(*a*). The spectrum shown in this figure was calculated from the turbulent signal recorded just before the transition. Figure 10(*b*) shows a spectrum and wave-form of the re-emergent periodicity after a few more steps in *Ra*. Note how much more developed the harmonics of f_2 are in this spectrum. The second harmonic $2f_2$ is only about 10 dB below f_2, whereas $2f_1$ was nearly 30 dB below f_1 in the initial periodic region (see figure 9*a*). This seems to indicate more nonlinearity at the higher Rayleigh numbers. The peak marked A* near the $4f_2$ harmonic is an aliased peak corresponding to the aliased fifth harmonic of f_2.

The spectrum of figure 10(*d*) shows a period-doubling bifurcation as reflected by the emergency of a peak at $\frac{1}{2}f_2$ and its multiples. The wave-form also displays the characteristics of a period-doubling bifurcation.

A slow modulation at frequency f_m* appears in the spectrum of figure 10(*d*), producing closely spaced sidebands of the fundamentals. The small modulation

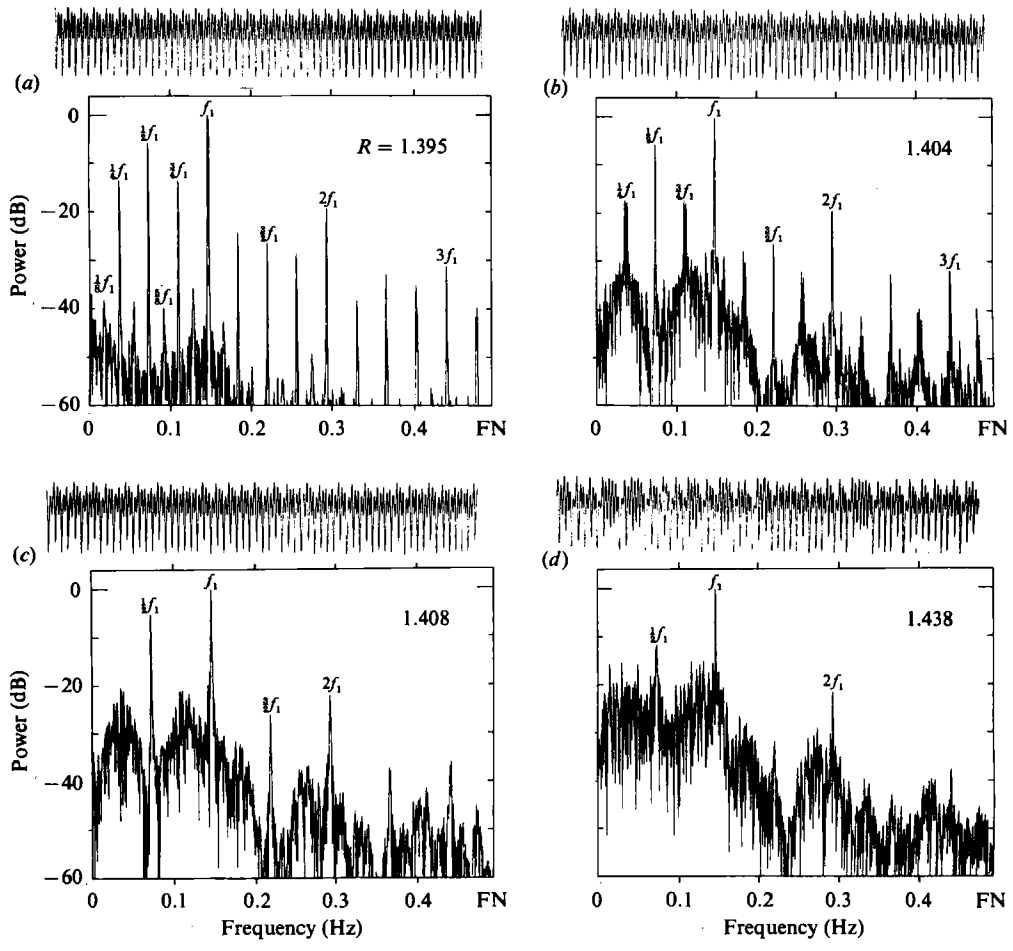

FIGURE 12. Selected power spectra and associated sections of recorded waveform, from sensor-perturbed up scan.

envelope can also be discerned in the waveform. The fundamental peaks appear to be slightly broadened at this Rayleigh number.

In figure 10(*e*), another unknown frequency f_u* appears at about the same frequency as f_u of the first periodic region. All peaks have become considerably broadened, indicating that the oscillations are becoming noisy. Sidebands from f_u* are evident as well as the slow modulation at frequency f_m*. The waveform has become considerably more complex, yet it still appears to be periodic.

At $R = 1.402$ the spectrum is fully broadband and the waveform is obviously noisy, as shown in figure 10(*f*). This turbulence persists up to $R = 1.80$, the maximum R obtainable in our experiment.

The down-scan was started at $R \approx 1.80$ where the up-scan concluded. The spectra are virtually identical with those of the up scan in the second periodic window (see Abernathey 1982). The spectra of the down scan remain periodic at frequency f_2 as R is decreased through this region. However, at approximately $R = 1.313$ (where weak turbulence began in the up scan) modulation of $f_2 + f_m = f_1$ eventually becomes larger than f_2. The modulation evidently provides a mechanism for smoothly switching between the two 'stable' modes f_2 and f_1. At $R = 1.270$, f_2 is still the

dominant peak, with several sharp sidebands and harmonics present. A small noisy peak f_u is also discernible. At $R = 1.268$, however, the f_1 peak dominates, indicating that the 'modes' have switched. The bases of the main peaks are broadened and there is a noisy band around f_u. The modulation quickly disappears with further decrease in Ra, and, as previously mentioned, the f_1 oscillation disappears at $Ra \approx 1.20$.

3.2.3. *Effect of thermal perturbation by sensors*

Since an intrusive measurement technique was used in the above experiments one must ask whether the observed convection behaviour was conditioned by the sensors. The unperturbed steady-state solutions (flow modes) are cylindrically symmetric about the axis of the cavity. However, in all runs we obtain essentially the same $2T'$ at a given Ra. This indicates that, probably because of the sensor–flow interaction, the 'rotational degeneracy' of the flow was lifted and, for example, the maximum flow velocities occurred always in the same vertical plane. The question remains whether, besides such a loss of a degree of freedom, the sensors may have caused a fundamental alteration of the flow. This was tested by changing the Joule heating in the sensors. The up–down scans were performed with a power dissipation of about 1 μW at each thermistor. Yet when the thermistor-probe bridge circuits were operated with a higher excitation voltage, resulting in a dissipation of approximately 50 μW, a fundamentally different route to turbulence was observed. The excess heat originating in the sensor is only partially dissipated by thermal conduction through the leads. Hence partial dissipation through – i.e. nonlinear coupling to – the convection mode is inevitable. This makes a quantitative estimate of the perturbation difficult. A systematic investigation of the sensor power threshold at which the convection behaviour described above was significantly altered would have been too time-consuming. But we feel that the 1 μW condition was safely within the realm of the above 'unperturbed' scenario.

Mostly as a warning for future experimentation and as an illustration of the possible consequences of *minor* sensor perturbations, we will briefly present the salient features of the convection behaviour obtained under the 50 μW condition. The bifurcation diagram shown in figure 11 summarizes the Ra-dependence of the major spectral features. The general appearance of this diagram is similar to that of the up scan: there is a weakly turbulent region separating the first periodic regime from the periodic window. Note that in this sequence $Ra^{osc} = 1280$, rather than 1550 as in the up scan. However, in this scan three period-doubling bifurcations were observed before the weak turbulence develops. Note that the R-spacing between successive period-doubling bifurcations decreases.

A spectrum and waveform of the third period-doubling bifurcation is shown in figure 12 (*a*). Although the waveform is complex, it is strictly periodic, repeating itself after eight cycles of the fundamental frequency. (It appears that the repetition takes only four cycles, but since the $\frac{1}{8}f_1$ peak is about 25 dB below $\frac{1}{4}f_1$ its effect is not readily discernible.) Figures 12 (*b*, *c*) present the spectra and waveforms obtained after two and three ΔR steps respectively from the R-value of figure 12 (*a*). The band-merging ($\frac{1}{4}f_1$ doublet) and noise rise in figure 12 (*b*) is characteristic of a 'strange attractor' (Farmer 1981; Crutchfield *et al.* 1980). The waveforms of figures 12 (*b*, *c*) are very similar to the periodic waveform of figure 12 (*a*), but one can see that they are no longer strictly periodic. The waveform becomes more non-periodic as R is increased, and all peaks but f_1 and a remnant of $\frac{1}{2}f_2$ disappear in the noise, as shown in figure 12 (*c*).

5. Summary

Differential scanning thermometry as employed in these experiments is a sensitive technique for determining transitions in steady-state free convective gas flow. We have determined the Rayleigh numbers for the onset of convection ($Ra^{cr} \approx 200$), a region of bistability ($400 \lesssim Ra \lesssim 700$) and the onset of time-dependent convection ($Ra \lesssim 1550$) for a cylinder of gas heated from below. The region of bistability was not reported in previous work with this system (Mitchell & Quinn 1966; Olson & Rosenberger 1978*a*, *b*). However, bistability of steady-states has been predicted theoretically (Rosenblat 1982) and experimentally demonstrated for a similar convection system at $Ra = 3.4$–$3.5\ Ra^{cr}$ (Behringer & Ahlers 1982).

Single-ended scanning thermometry combined with digital signal-processing techniques was used to study the dynamical nature of time-dependent convection. In the up scan (see figure 7) slightly supercritical time-dependent convection is strictly periodic (frequency f_1). As Ra is increased, a second incommensurate frequency f_2 develops, producing quasiperiodicity. A third frequency f_u appears just before the onset of weak turbulence. This weak turbulence is *intermittent*, i.e. quasiperiodic intervals are separated by intervals of chaotic behaviour. As Ra is increased further, a periodic window re-emerges from turbulence. The frequency f_2 of this oscillation is apparently related to the band at lower Ra (below the weakly turbulent region). Further Ra-increases induce a f_2 period-doubling bifurcation, which is immediately followed by fully developed turbulence. The route from turbulence to periodicity is not a mirror image of the route from periodicity to turbulence. The most notable differences in the down scan are the absence of a weakly turbulent region at intermediate Ra and a recovery to steady-state behaviour at Ra above the onset of time-dependence in the up scan.

Self-heating of the temperature-sensing probes alters the dynamical behaviour by coupling the measurement process to the thermally convecting gas. Time-dependence sets in at a lower Ra^{osc}, and is initially periodic at a lower frequency f_1. As Ra is increased, a cascade of period-doubling bifurcations is induced. Subharmonics as low as $\frac{1}{8}f_1$ are resolvable before non-periodicity develops. Thus turbulence is characterized by a merging of subharmonics into chaotic bands. For a range of Ra sharp spectral peaks at f_1 and its sub- and higher harmonics persist in an otherwise noisy spectrum. These peaks eventually disappear into noise at higher Ra. At still higher Ra periodicity re-emerges over a narrow window of Ra. Within this window a variety of quasiperiodic behaviour is observed before turbulence redevelops.

6. Conclusions

Although the flow underlying the observed phenomena is not entirely clear, recent interest in nonlinear instabilities and transitions has provided a framework for examining our results (see e.g. Velarde 1981; Eckmann 1981).

Neither of the routes to chaos we observed support the Landau–Hopf picture of turbulence. Both routes clearly demonstrate that a small number of bifurcations to periodic states precede the onset of chaotic flow. Most other experimental work also supports this conclusion (Gollup 1983).

The development of quasiperiodicity with three incommensurate frequencies (up scan) is consistent with the Ruelle–Takens picture of the transition to turbulence. Essentially the same route has been observed for convection systems with much

smaller height-to-radius ratios (Dubois & Berge 1980; Gollub & Benson 1980; Maurer & Libchaber 1979).

Although intermittency did not provide a *route* to turbulence in our system, it is clearly associated with the onset of weak turbulence in the up scan.

The cascade of period-doubling bifurcations in the period-doubling-bifurcation scan supports the Feigenbaum picture of turbulence. Although much of the work demonstrating the Feigenbaum scenario is based on the dynamics of very simple one-dimensional nonlinear systems (May 1976), a Feigenbaum route to turbulence is also known to occur in solutions to the Navier–Stokes equations including thermosolutal convection (Moore *et al.* 1983). Several other experiments have also produced Feigenbaum sequences (Koster & Müller 1982; Gollub & Benson 1980; Giglio 1982). The merging of subharmonics into 'strange' bands (Farmer 1981; Crutchfield *et al.* 1980) (figures 12*b–c*) is also characteristic of the Feigenbaum scenario; however, we are not aware of any other convection experiments that show this feature.

The re-emergence of periodic windows from chaos is another feature our experiments have in common with simpler nonlinear systems that undergo period-doubling bifurcations (May 1976; Moore *et al.* 1983). Although we are not aware of re-emergent periodicity in other thermal convection experiments, it has been observed in Taylor–Couette flow (Walden & Donnelly 1979). Since many nonlinear systems have several periodic windows imbedded in chaotic regions (May 1976; Moore *et al.* 1983; Abernathey 1982) we expect the existence of more such windows in free convective turbulence at *Ra*-values beyond the range investigated here.

This work was supported by NSF Grant DMR 79-13183.

REFERENCES

Abernathey, J. R. 1982 Thermal convection of gases in cylindrical containers. Ph.D. dissertation, University of Utah.

Behringer, R. P. & Ahlers, G. 1982 Heat transport and temporal evolution of fluid flow near the Rayleigh–Bénard instability in cylindrical containers. *J. Fluid Mech.* **125**, 219–258.

Brigham, E. O. 1974 *The Fast Fourier Transform.* Prentice-Hall.

Crutchfield, J., Farmer, D., Packard, N., Shaw, R., Jones, G. & Donnelly, R. J. 1980 Power spectral analysis of a dynamical system. *Phys. Lett.* **76A**, 1–4.

Dubois, M. & Bergé, P. 1980 Experimental evidence for the oscillators in a convective biperiodic regime. *Phys. Lett.* **76A**, 53–56.

Eckmann, J.-P. 1981 Roads to turbulence in dissipative systems. *Rev. Mod. Phys.* **53**, 643–654.

Farmer, J. D. 1981 Spectral broadening of period-doubling bifurcation sequences. *Phys. Rev. Lett.* **47**, 179–182.

Feigenbaum, M. J. 1979 The onset spectrum of turbulence. *Phys. Lett.* **74A**, 375–378.

Giglio, M. 1982 Transition to chaotic behaviour via period doubling bifurcations. *Appl. Phys.* **B28**, 165.

Gollub, J. P. & Benson, S. V. 1980 Many routes to turbulent convection. *J. Fluid Mech.* **100**, 499–470.

Gollub, J. P. 1983 In *Nonlinear Dynamics and Turbulence.* (ed. G. I. Barenblatt, G. Iooss & D. D. Joseph). Pitman.

Hirsch, J. E., Huberman, B. A. & Scalapino, D. J. 1982 Theory of intermittency. *Phys. Rev.* **A25**, 519–532.

HIRSCH, M. W. & SMALE, S. 1974 *Differential Equations, Dynamical Systems, and Linear Algebra.* Academic.

KOSTER, J. N. & MÜLLER, V. 1982 Free convection in vertical gaps. *J. Fluid Mech.* **125**, 429–451.

LANDAU, L. D. & LIFSHITZ, E. M. 1978 *Fluid Mechanics.* Pergamon.

L'VOV, V. S. & PREDTECHENSKY, A. A. 1981 On Landau and stochastic attractor pictures in the problem of transition to turbulence. *Physica* **2D**, 38–51.

MARSHALL, J. L. 1965 *Introduction to Signal Theory.* International Textbook Company.

MAURER, J. & LIBCHABER, A. 1979 Rayleigh–Bérnard experiment in liquid helium; frequency locking and the onset of turbulence. *J. Physique Lett.* **40**, L419–L423.

MAY, R. M. 1976 Simple mathematical models with very complicated dynamics. *Nature* **261**, 459–467.

MITCHELL, W. T. & QUIN, J. A. 1966 Thermal convection in a completely confined fluid layer. *A.I.Ch.E. Jl.* **12**, 1116–1124.

MOORE, D. R., TOOMRE, J., KNOBLOCH, E. & WEISS, N. O. 1983 Period doubling and chaos in partial differential equations for thermosolutal convection. *Nature* **303**, 663–667.

NORMAND, C., POMEAU, Y. & VELARDE, M. G. 1977 Convective instability: a physicists approach. *Rev. Mod. Phys.* **49**, 581–624.

OLSON, J. M. & ROSENBERGER, F. 1978*a* Convective instabilities in a closed vertical cylinder heated from below. Part 1. Monocomponent gases. *J. Fluid Mech.* **92**, 609–629.

OLSON, J. M. & ROSENBERGER, F. 1978*b* Convective instabilities in a closed vertical cylinder heated from below. Part 2. Binary gas mixtures. *J. Fluid Mech.* **92**, 631–642.

POMEAU, Y. & MANNEVILLE, P. 1980 Intermittent transition to turbulence in dissipative dynamical systems. *Commun. Math. Phys.* **74**, 189–197.

RABINER, L. R. & GOLD, B. 1975 *Theory and Application of Digital Signal Processing.* Prentice-Hall.

ROSENBLAT, S. 1982 *Thermal convection in a vertical circular cylinder. J. Fluid Mech.* **122**, 395–410.

RUELLE, D. & TAKENS, F. 1971 On the nature of turbulence. *Commun. Math. Phys.* **20**, 167–192.

SWINNEY, H. H. & GOLLUB, J. P. (eds) 1981 *Hydrodynamic Instabilities and the Transition to Turbulence.* Springer.

VELARDE, M. G. 1981 Steady states, limit cycles and the onset of turbulence. A few model calculations and exercises. In *Nonlinear Phenomena at Phase Transitions and Instabilities* (ed. T. Riste), pp. 205–247.

WALDEN, R. W. & DONNELLY, R. J. 1979 Reemergent order of chaotic circular Couette flow. *Phys. Rev. Lett.* **42**, 301–304.